AFRL-RV-PS-
TR-2016-0068
AFRL-RV-PS-
TR-2016-0068

PLASMA PHYSICS OF THE SUBAURORAL SPACE WEATHER

Evgeny V. Mishin, et al.

20 March 2016

Final Report

AIR FORCE RESEARCH LABORATORY
Space Vehicles Directorate
3550 Aberdeen Ave SE
AIR FORCE MATERIEL COMMAND
KIRTLAND AIR FORCE BASE, NM 87117-5776

DTIC COPY

NOTICE AND SIGNATURE PAGE

AFRL-RV-PS-TR-2016-0068 HAS BEEN REVIEWED AND IS APPROVED FOR PUBLICATION IN ACCORDANCE WITH ASSIGNED DISTRIBUTION STATEMENT.

//SIGNED//	//SIGNED//
Dr. Evgeny Mishin	Glenn M. Vaughan, Colonel, USAF
Project Manager, AFRL/RVBXI	Chief, Battlespace Environment Division

REPORT DOCUMENTATION PAGE

Form Approved
OMB No. 0704-0188

1. REPORT DATE *(DD-MM-YYYY)*	2. REPORT TYPE	3. DATES COVERED *(From - To)*
20-03-2016	Final Report	01 Oct 2013 to 30 Sep 2015

4. TITLE AND SUBTITLE
Plasma Physics of the Subauroral Space Weather

5a. CONTRACT NUMBER

5b. GRANT NUMBER

5c. PROGRAM ELEMENT NUMBER
61102F

6. AUTHOR(S)
Evgeny V. Mishin, Vladimir Sotnikov, and Eric Sutton

5d. PROJECT NUMBER
3001

5e. TASK NUMBER
PPM00016891

5f. WORK UNIT NUMBER
EF122002

7. PERFORMING ORGANIZATION NAME(S) AND ADDRESS(ES)
Air Force Research Laboratory
Space Vehicles Directorate
3550 Aberdeen Ave SE
Kirtland AFB, NM 87117-5776

8. PERFORMING ORGANIZATION REPORT NUMBER
AFRL-RV-PS-TR-2016-0068

9. SPONSORING / MONITORING AGENCY NAME(S) AND ADDRESS(ES)

10. SPONSOR/MONITOR'S ACRONYM(S)
AFRL/RVBXI

11. SPONSOR/MONITOR'S REPORT NUMBER(S)

12. DISTRIBUTION / AVAILABILITY STATEMENT
Approved for public release; distribution is unlimited. (OPS-16-10852 dtd 29 Mar 2016)

13. SUPPLEMENTARY NOTES

14. ABSTRACT
This research addresses basic plasma processes that control the dynamics of the perturbed inner magnetosphere/subauroral ionosphere termed the subauroral geospace. Our observations demonstrated the need of a dramatic re-evaluation of our understanding of the development of the subauroral disturbances. Using multispacecraft observations near the magnetic equator and in the ionosphere, we specified their features and space weather effects. Near substorm onsets, highly irregular subauroral regions create strong scintillations of UHF and GPS L1 band signals. Irregular structures in the plasmasphere guide VLF whistler waves thereby facilitating precipitation of radiation belt electrons. Our study shows that the conventional 30-year paradigm is in serious error and so puts forward a novel concept of a turbulent plasmaspheric boundary layer formed in the evening sector where the plasmasphere short-circuits reconnection-injected hot plasma jets. To describe UHF/GPS L1 band irregularities, a numerical, first-principle hybrid model of interchange and Kelvin-Helmholtz instabilities in the equatorial and midlatitude ionosphere has been developed. It includes finite Larmor radius effects in low (ionosphere) and high (plasma sheet) beta plasmas with velocity shear to go beyond the state-of-the-art fluid models, e.g. AFRL/PBMOD.

15. SUBJECT TERMS
subauroral ion drifts, substorm-injected plasma jets, SAID/SAPS-related plasma waves, plasmaspheric boundary layer

16. SECURITY CLASSIFICATION OF:			17. LIMITATION OF ABSTRACT	18. NUMBER OF PAGES	19a. NAME OF RESPONSIBLE PERSON
a. REPORT	b. ABSTRACT	c. THIS PAGE			Dr. Evgeny Mishin
Unclassified	Unclassified	Unclassified	Unlimited	20	19b. TELEPHONE NUMBER *(include area code)*

This page is intentionally left blank.

Table of Contents

List of Figures

1. SUMMARY

Subauroral magnetic field lines map to the inner magnetosphere, including the ring current (RC), outer radiation belt (RB), and plasmasphere earthward of the electron plasma sheet boundary (the auroral boundary in the ionosphere). During space storms, the inner edge of the RB electrons follows the perturbed plasmasphere' s boundary (the plasmapause, PP), while the plasma sheet (PS) electron and ion boundaries significantly separate. Energetic ions form the perturbed ring current. In turn, channels of intense, poleward directed electric fields develop in the subauroral geospace creating jets of enhanced westward convection termed Sub-Auroral Ion Drifts (SAID) and Sub-Auroral Polarization Streams (SAPS). Observations indicate SAID/SAPS as the most prominent feature of the perturbed subauroral geospace. The subauroral region is among significant contributors to space weather due to distinct electromagnetic and plasma structures and turbulence within SAPS [1, 2]. These result in precipitating RC protons and RB electrons, high TEC gradients, and strong scintillations of UHF and L-band signals. Besides mid-latitude scintillations, the SAPS-type subauroral processes are also closely tied to generation of storm enhanced densities and creation of polar cap patches, which are the primary driver of scintillation in the high-latitude region. The development of subauroral spatial-temporal variability is among the hottest space weather topics.

This research aims at attaining the required level of understanding of the SAID/SAPS generation mechanisms. The objectives are to characterize, and understand basic plasma processes that control the subauroral geospace dynamics/structure. These include: (1) the interaction of substorm-injected plasma with the plasmasphere that forms a plasmaspheric boundary layer and creates SAID/SAPS, (2) the generation of SAID/SAPS-related plasma waves, and (3) the development of a numerical, first-principle hybrid model of interchange and Kelvin-Helmholtz instabilities in the midlatitude ionosphere which includes finite Larmor radius effects. The results advance the understanding of the physics underlying the spatial-temporal development of the perturbed subauroral geospace and pertinent space weather effects.

2. INTRODUCTION

During last three decades the paradigm of voltage and current generators based on the test (single) particle approach dominated the subauroral geospace research. The former places SAID/SAPS between the inner boundaries of ≥1-keV ion and electron convection defined by the **E×B** and gradient and curvature drifts. However, this approach violates the plasma quasi-neutrality, intrinsic of slow processes. The current generator explores closure of the Region 2 field-aligned current (FAC) through a low-conductive ionosphere, resulting in locally enhanced poleward electric field E_s. The generators' concept have come to be called the SAID/SAPS paradigm. It predicts that the ring current and SAID/SAPS are built upon a slow, a few hours, timescale. The corollary to the above is that SAID/SAPS should follow the asymmetric RC development and be enclosed by the R2 and R1 FACs. However, our earlier results [3] demonstrate that this paradigm is in serious error and cannot explain the spatial-temporal variability in the region of interest.

One of the most striking discrepancies is that substorm subauroral events appear in ~10 min or less. Figure 1 exemplifies such events from the DMSP F14 satellite that appear in less than 10

minutes after the onset of the substorm expansion phase [4, 5]. From top to bottom are the downcoming electron and ion differential fluxes in the range of 0.03-30 keV, horizontal plasma drifts, electron and ion temperatures, and plasma densities.

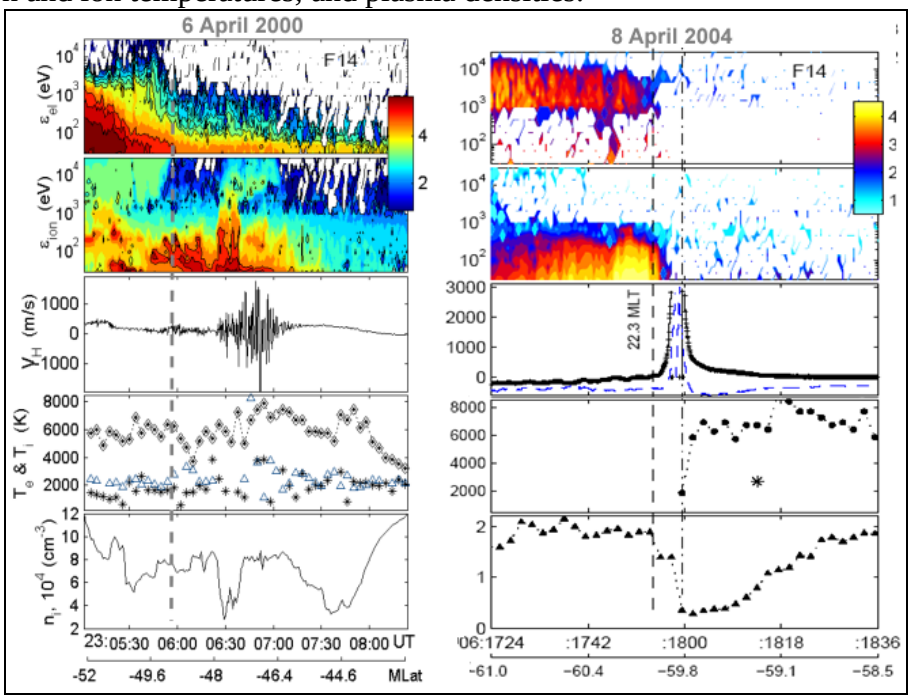

Figure 1. DMSP F14 observations of fast time (left) SAPS and (right) SAID events

As the fast timescale is characteristic of propagation of substorm injection fronts, we focus on the observations near substorm onsets (see sections 3.1 and 4.1).

Ionospheric scintillation, a key component of the Space Weather, disrupts communication, navigation, and surveillance systems [6]. Scintillations in the UHF and GPS L-band channels are caused by small-scale ionospheric irregularities with transverse scale lengths <100 m. Strong UHF/GPS scintillations observed within the SAPS region indicate the presence of such irregularities [2]. As the state-of-the-art fluid models, e.g. AFRL/PBMOD [7], are incapable of predicting small-scale structures less than 1 km, it is necessary to go beyond the fluid approximation and include ion kinetic effects. Therefore, we develop a numerical, physics-based hybrid model which includes finite Larmor radius effects and thus capable of describing small-scale irregularities (see sections 3.2 and 4.2).

3. METHODS, ASSUMPTIONS, AND PROCEDURES

3.1 Selection of events

The Kyoto WDC quicklook auroral indices AU/AL and AE and the IMAGE database [8] are analyzed to specify the development of substorms. Then, we use the AFRL database of DMSP and GRACE/CHAMP and the NASA Goddard database of Cluster, Polar, and CRRES to obtain key ionosphere/thermosphere and inner magnetosphere data, respectively. The main initial tusk is to identify events near the magnetic equator following the onsets of substorms and

magnetically conjugate with those in the ionosphere. After such events are identified, they are explored to establish the SAID/SAPS salient features.

3.2 Tuning a hybrid code with ion kinetic effects to ionosphere

The AFRL high-resolution code "Flute" [9] was originally aimed at interchange instabilities in high-beta, high energy plasmas. To apply it to the midlatitude ionosphere, a system of nonlinear equations is derived for description of the plasma instabilities resolving spatial scales down to ~10 m, as needed to describe scintillations of the UHF and GPS L-band signals. Numerical solutions provide spectra of developed turbulence for various combinations of the known driving forces, including velocity shears, neutral winds, and penetrating electric fields. Validation of the results starts comparing with the large-scale fluid modeling by turning-off the kinetic effect. The ultimate validation of the model should be achieved by comparing the high-resolution spectra with those revealed from the high-resolution in situ observations.

4. RESULTS AND DISCUSSION

4.1 Observations of substorm SAID/SAPS

Overall, more than 40 substorm events in both hemispheres with the time span after the substorm onset ranging from 10 min to 2 hours and during major storms have been explored to establish the SAID/SAPS salient features [10-13]. Figure 2 exemplifies the SAID events we focused on during this work. Shown are the SAID channels after the onset of a substorm [8] near L = 6.8 and 22.9 MLT at 09:47:35 UT on 18 March 2002. Left frame displays the meridional electric field (not to scale) from the Cluster 1 satellite during inbound (the southern hemisphere) and outbound (northern) passes (C1 at an altitude h~25000 km) in the meridional plane at 23.0 MLT, with the positions of Polar (h~5500 km) and DMSP F14 (h~850 km) indicated. Dipolar magnetic field lines are shown for reference. The thick arrow indicates an oncoming substorm-injected plasma jet (plasmoid). Right frame: (top) Meridional (outward) electric fields in mV/m; (2^{nd} row) H+ differential number fluxes (the dashed curve shows the potential energy $e\Delta\Phi$ calculated from the measured electric field); (3^{rd}) C1 1-keV electron counts and Polar/F14 electron fluxes; (bottom) the plasma densities. Color codes are in logarithmic scale.

Apparently, there are two magnetically conjugate groups: Cluster - F14 in the southern hemisphere and Cluster - Polar in the northern hemisphere. The Cluster and Polar electric fields mapped into the ionosphere match that from F14 to within ~10%. The hot electron population at Polar closely resembles that mapped from DMSP, and the 1-keV electron flux scales to Cluster's 1-keV electron counts. The SAID's outer side is aligned with PP, while the inner edge co-locates with the sharp decrease of the hot ion flux. The obvious corollary is that the SAID channel is inside the plasmasphere devoid of the hot PS electrons. Further, the test-particle approach predicts that the auroral boundary follows drift trajectories of (test) keV electrons so that their maximum energy gradually decreases inward. However, this disagrees with the in situ data during the SAID events. Apparently, the hot electron boundary is coincident with the density increase on the plasmapause and represents an abrupt dispersionless cutoff.

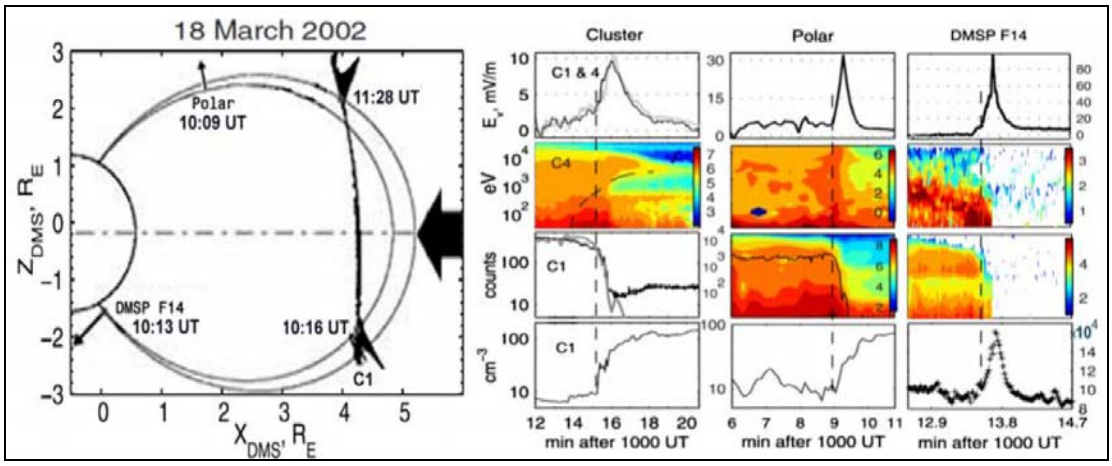

Figure 2. The 18 March 2002 Cluster/Polar/DMSP SAID event

We emphasize that this type of the substorm auroral boundary remained a mystery since its discovery [14]. Namely, the dispersionless nature of the hot electron cutoff and its dependence on the cold plasma density exclude the usual (test particle) Alfvén layer interpretation. Nor can the test-particle "nose" distribution of westward-drifting energetic ions fit the observed hot ion distribution within the SAID channel. By the same token, the generator paradigm cannot explain the size of the SAID channel in terms of the Alfvén layer. However, these features follow directly from the concept of a turbulent plasmaspheric boundary layer (see section 4.2).

Figure 3 shows the related magnetic variations (2nd row) and currents (3rd row) for the SAID events on 18 March 2002 and 8 April 2004 [cf., 10, Figures 6-8].

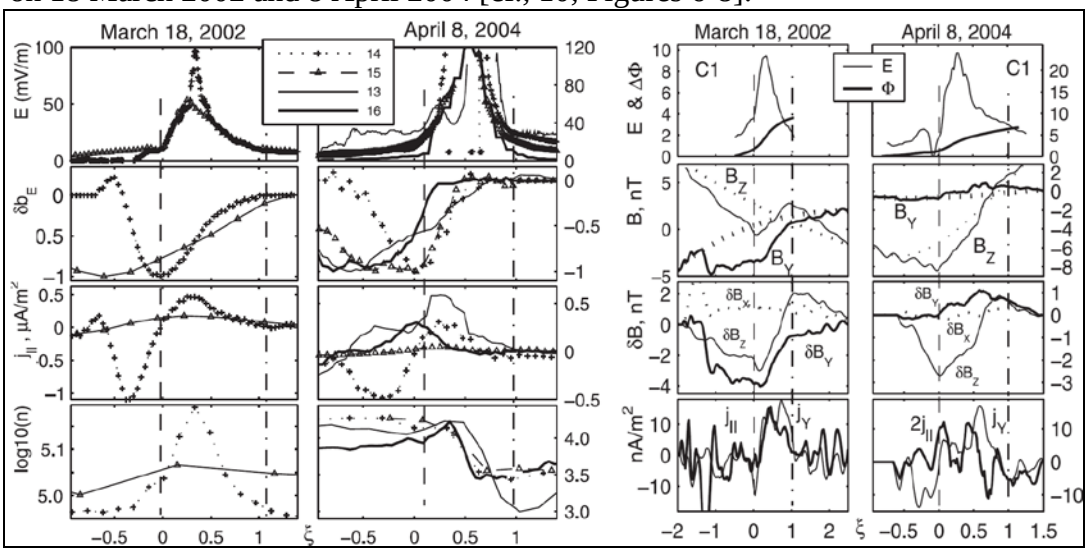

Figure 3. SAID-related current systems

Apparently, the downward FACs in the ionosphere concentrate near the SAID's outer/poleward boundary. In the magnetosphere, the downward FACs near the outer edge ($\xi = 0$) virtually mimic ionospheric counterparts. However, FAC's magnitude at Polar is close to that mapped from DMSP but twice as smaller as that mapped from Cluster. This substantial difference and the lack of the ionospheric counterpart of the inner, alternating part of the magnetospheric current

indicate partial closure of the downward FAC above Polar (>5500 km). Note also that no density trough is present in the ionosphere (4th row). That is, contrary to the current generator paradigm, neither the field-aligned currents enclose the SAID channel nor the plasma density (conductivity) minimizes in the SAID region.

The overall dataset [3, 5, 10-13] shows that the generator paradigm is in serious error. Therefore, we put forward a concept of the SAID channel as an integral part of a turbulent plasmaspheric boundary layer (TPBL) formed in the evening sector where the plasmasphere short-circuits reconnection-injected hot plasma jets.

4.2 Turbulent Plasmaspheric Boundary Layer

In agreement with the three-decade statistics [e.g., 15], the explored fast time SAID events concentrate in the premidnight MLT sector, characteristic of the propagation of substorm injections. We consider near-tail substorm-injected ($H^+ - e$) plasma jets as hot plasma jets of the cross-tail width a moving with the bulk speed $\mathbf{v}_0 \| \mathbf{x}$ across the magnetic field $\mathbf{B}_\perp(x) \| \mathbf{z}$. This system of reference is close to GSM near the magnetic equator and midnight. The magnetic pressure in the inner magnetosphere usually greatly exceeds the ram pressure of the injected plasma jets. Accordingly, infinite-width jets will be halted near the source. However, jets of limited a (hereafter, plasmoids) can propagate across magnetic barriers can penetrate magnetic barriers owing to self-polarization fields formed at the front. For that their density N_h must exceed $N_{min} \approx 0.3(B_\perp/400)^2$ cm^{-3}, where $B_\perp$ is in nT (see details and references in [10]). In the events of interest, a typical upstream hot ion density $N_h \approx$ 1-2 cm^{-3} amonts to $\approx(3\text{-}6)N_{min}$.

However, this self-similar motion breaks as soon as the surrounding plasma shorts out the polarization field at the front. This occurs at the plasmapause when the cold plasma density exceeds the critical value ~10 cm^{-3}. As a result, the hot electrons come to a halt, thereby forming the dispersionless plasma sheet/auroral boundary. In the plasmasphere devoid of the hot electrons, the cold plasma maintains quasi-neutrality. This is a short circuit of a hot plasmoid over the cold plasma. The hot ions yet move inward over the distance ~$(0.1\text{-}0.2)R_E$ until being halted by the emerging SAID electric field.

Therefore, the SAID channel can be pictured as a turbulent plasmaspheric boundary layer with an unstable mixture of the hot ion and cold plasma populations. The critical role of plasma turbulence for the SAID formation is to provide anomalous resistivity in the circuit and magnetic diffusion. Save the short-circuiting and plasma turbulence effects, quite similar approach is used for understanding impulsive plasma penetration of the dayside magnetopause.

Let explore the wave activity accompanied the events in question, alike the SAPS events [e.g., 1]. Figure 4 presents electric (mV^2/m^2Hz) and magnetic (nT^2/Hz) wave components from Cluster coincident with the above SAID events [cf., 10, Figure 4]. Horizontal lines on the frequency-time spectrograms indicate the lower hybrid resonance (solid) and the tenth, fourth, and second harmonics (dashed) of the H+-ion gyrofrequency ~5.4 Hz, derived from the observed magnetic field. It is seen that the wave activity is greatly enhanced inside the SAID channel. Intense broadband waves arise in the entry layer of the thickness ~90 km near the outer boundary and extend to the center. The waves in the entry layer are mainly electrostatic ion cyclotron/Bernstein

(ICB) and lower hybrid (LH) modes, while highly oblique electromagnetic whistler (W) and fast magnetosonic (MS) waves appear near and earthward of the E_s peak.

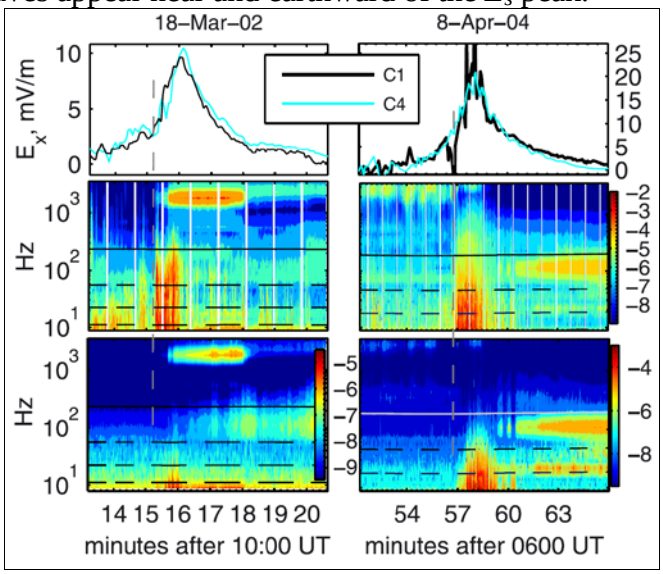

Figure 4. SAID-associated plasma waves

Figure 5 gives more details of the 18 March 2002 southern SAID. From top to bottom are (a) the C1 outward and scaled eastward electric components, (b) H^+ differential omnidirectional number fluxes in the range 1-10 eV, (c) the r.m.s. amplitudes of the electrostatic waves in the lower hybrid (LH), magnetosonic (MS), whistler (W) bands, (d) the perpendicular hot ion (electron) pressure $P_{i,e}$, density N_i and ion anisotropy $\delta T = T_\perp/T_\parallel - 1$, (e) deviations from the model field of the observed, $\Delta B = B - B_0$ (the thick line), and the `inner' or downstream, $\Delta B_d^{ext} = B_d^{ext} - B_0$ (dashed), magnetic fields; as well as the diamagnetic correction ΔB_{i+e}^{dia}. Here ΔB_d^{ext} is obtained by a polynomial fit of the magnetic field downstream of the channel (at >10:18:10 UT) and extrapolated upstream.

Upstream of the channel, we have taken $P_{i+e}=P_I+P_e \approx (3/2)P_i$ (the hot ion pressure from Cluster) by extrapolating the Polar/HYDRA data. The excellent matching of ΔB_{i+e}^{dia} with the observed ΔB upstream of the channel (at <10:15:10 UT) indicates the permeation of the incoming hot plasma by the downstream field (due to anomalous magnetic diffusion). This agrees with the value of the effective collision frequency due to wave-particle interactions calculated with the observed turbulent fields [10]. However, ΔB_{i+e}^{dia} significantly deviates from ΔB near the outer boundary, especially in the entry layer. Accordingly, the presumed diamagnetic current (positive eastward) is opposite to the observed one. This discrepancy comes is due to our assumption that the extrapolated relation $P_e \approx (1/2)P_i$ upstream of the SAID channel is still valid inside the channel. However, while the hot ions move farther inward, the hot electrons should accumulate about their cutoff boundary. In a steady state, this accumulation is balanced via precipitation and azimuthal drift. The conjugate (Polar and DMSP) hot electron precipitation shows no noticeable increase near the boundary. Therefore, the azimuthal (diamagnetic) drift is the prime contender thereby giving the observed westward current in the entry layer [10].

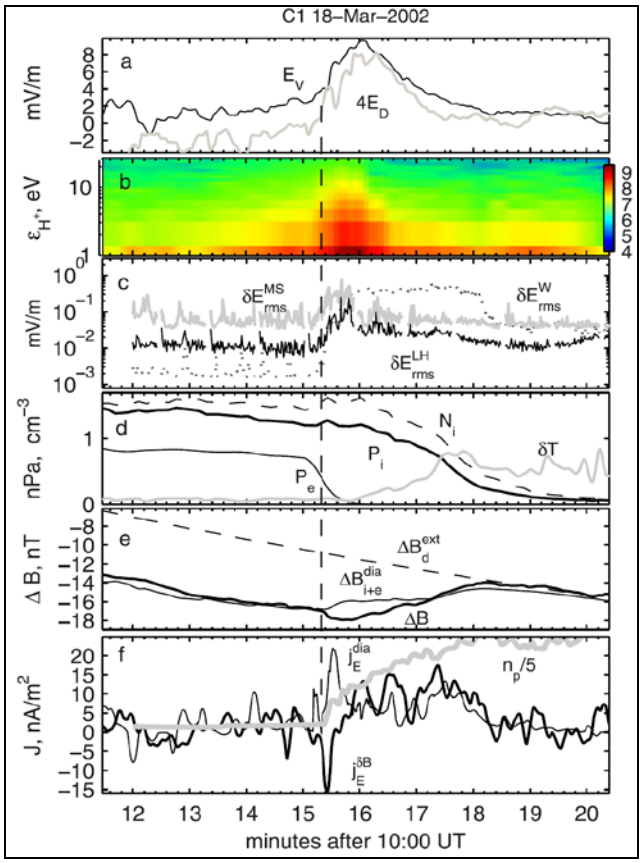

Figure 5. Fine structure of the SAID channel

It is readily seen that the suprathermal ion population is coincident with enhanced wave activity in the channel, and ~1-eV ions extend also up- and down-stream. Note that in the entry layer MS means the ICB waves. As shows panel d, the inner SAID boundary corresponds to the drop of P_i and N_i to ≈0.3 nPa and 0.4 cm^{-3}, respectively, i.e. by a factor of 4, which is consistent with the value of N_{min}. As the hot ion anisotropy increases across the channel, $\delta T \approx 0.1 \rightarrow 0.8$, the ($\perp B$) ion distribution reduces to the so-called ion-ring distribution, which is the main driver of the wave activity near the center of the channel and further inward. Note also that δE_{rms}^{W} downstream of the channel remains well above the upstream level. This observation is the key for explaining the relation of the outer RB boundary with the plasmapause earlier discussed in [16].

4.3 Physics-based hybrid model with finite Larmor radius effects

Strong UHF/GPS scintillations in the subauroral ionosphere indicate the presence of density irregularities with transverse scale lengths <100 m. As the state-of-the-art fluid models, e.g. AFRL/PBMOD, are incapable of predicting small-scale structures ~10s-100s of meters, it is necessary to go beyond the fluid approximation and include ion kinetic effects. A numerical, first-principle hybrid model of interchange and Kelvin-Helmholtz instabilities in the equatorial and midlatitude ionosphere has been developed [17-19]. Nonlinear system of equations describing the evolution of the interchange and Kelvin-Helmholtz (KH) instabilities in the

presence of finite Larmor radius effects in low- (ionosphere) and high-beta (plasma sheet) plasmas with velocity shear has been derived. It includes the combined effect of interchange and KH instabilities in 2D geometry in a plane perpendicular to an external magnetic field (||**Z**) with transverse (⊥X) inhomogeneity in plasma density and plasma flow (||**Y)**. The normalized system of collisionless fluid equations is as follows

$$\frac{\partial \Delta\delta\varphi}{\partial t} = -V_0 \frac{\partial \Delta\delta\varphi}{\partial y} + V_0^{''} \frac{\partial \delta\varphi}{\partial y} + \frac{T_i}{T_e} V_0^{'} \frac{\partial^2 \delta n}{\partial x \partial y} + \frac{T_i}{T_e} V_0^{''} \frac{\partial \delta n}{\partial y} + \frac{T_i}{T_e} \nabla \cdot \{\nabla \delta\varphi, \delta n\} - \{\delta\varphi, \Delta\delta\varphi\} + V_0^{'} \{\delta n, \delta\varphi\}, \tag{1}$$

$$\frac{\partial \delta n}{\partial t} = -V_0 \frac{\partial \delta n}{\partial y} + \{\delta n, \delta\varphi\}. \tag{2}$$

Equation (1) describes the evolution of the perturbed vorticity $\Delta\delta\varphi$, Eq. (2) describes the perturbed density δn, and $\delta\varphi$ is the first-order potential. Finite gyro-radius effects are captured through the terms that include the ratio of the electron to ion temperatures (T_e/T_i). Equations (1) and (2) are in dimensionless form, with time normalized by the ion cyclotron frequency Ω_{ci} and with spatial scales normalized by $\rho_s = V_s/\Omega_{ci}$, where $V_s = \sqrt{T_e/M_i}$ is the sound speed with M_i the ion mass. In Eqs. (1) and (2), $\Delta \equiv \nabla^2$, $V_0^{'} \equiv dV_0/dx$, and $V_0^{''} \equiv d^2V_0/dx^2$. The Poisson bracket operator is defined as

$$\{A, B\} \equiv \frac{\partial A}{\partial x}\frac{\partial B}{\partial y} - \frac{\partial A}{\partial y}\frac{\partial B}{\partial x}.$$

The *y*-directed sheared velocity function selected for this analysis is

$$V_0(x) = V_{0\max} \frac{x - x_0}{L} \exp\left[-\left(\frac{x - x_0}{L}\right)^2\right], \tag{3}$$

where $V_{0\max}$ is the peak velocity amplitude, L determines the gradient of the shear, centered at x_0.

Equations (1) and (2) are solved numerically on a uniform finite-difference grid in 2D (*x*,*y*). A 2D code previously developed for the analysis of flute-type unstable modes [9] has been adapted to solve the nonlinear equations. The spatial grid extends between $1 \le x, y \le 256,$ where *x* and *y* are normalized spatial dimensions, and $dx = dy = 1.$ Periodic boundary conditions are used in both directions. The equations are solved using a predictor-corrector scheme, with a fixed time step $dt = 0.5$ (normalized). Artificial damping and viscosity terms are used for numerical stability.

Linear perturbations of the quantities δn and $\delta\varphi$ of the form

$$\delta p \sim \delta p(x) \exp\left[i(ky - \omega t)\right], \tag{4}$$

are considered, where $\omega = \omega_r + i\gamma$ is the complex frequency with $\gamma > 0$ indicating linear instability. Substitution into Eq. (2) as dropping the nonlinear term shows that $\delta n \neq 0$ in the linear regime. From Eq. (1), again dropping the nonlinear Poisson bracket terms, the following second order differential equation for the linearly perturbed potential $\delta\varphi$ is obtained:

$$\frac{d^2\delta\varphi}{dx^2} - k^2\delta\varphi + \frac{kV_0^{"}}{\omega - kV_0}\delta\varphi = 0. \tag{5}$$

This equation is solved numerically on a 1D (x) grid using a standard shooting code with zero derivative $(d\delta\varphi/dx = 0)$ boundary conditions. Using $L = 32,\ x_0 = 129,$ and $V_{0\max} = 1,$ the numerical solution to Eq. (5) is found and used to obtain the growth rate as a function k. This result is shown in Figure 6(a) as the solid black curve. The red dot indicates the expected growth rate for the longest unstable wavelength that fits with the simulation box; $kL = 2\pi L/\lambda \neq 0.7854$. Figure 6(b) plots the spatially-averaged square of the potential $\left\langle (\delta\varphi)^2 \right\rangle$ on the grid as a function of time (solid black curve). The dashed red line is an approximate fit to the black curve and demonstrates that the calculated linear growth rate agrees well with that from dispersion analysis for the Kelvin-Helmholtz instability.

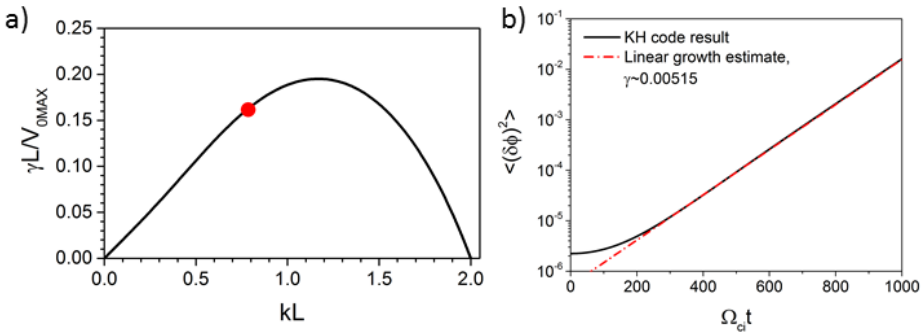

Figure 6. Linear dispersion analysis

Then, a 2D numerical code was run with these same parameters to obtain the linear growth of the Kelvin-Helmholtz instability and nonlinear saturation (Figure 7). The linear growth of the instability saturates due to the nonlinear interaction of different unstable modes in the system. During this phase, several of the nonlinear terms in Eqs. (1) and (2) provide coupling between the potential and density. Eventually, broad-spatial-spectrum density structures appear.

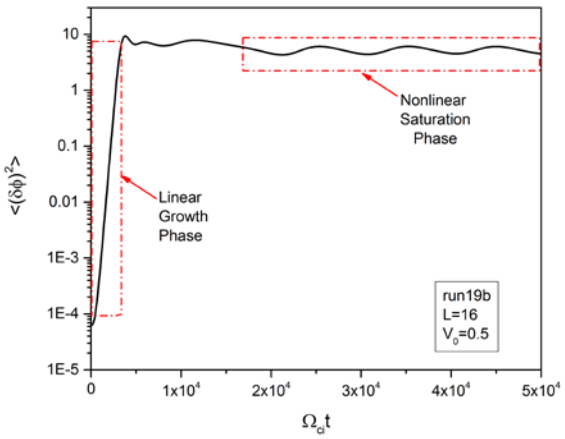

Figure 7. Time evolution of the potential

Figure 8 shows sample results for a code run with $V_{0\max} = 0.1$, $T_e/T_i = 1$, $L = 8$, and $x_0 = 129$. The averaged squared potential as a function of time is shown in Figure 8(a). The linear growth phase occurs in the first ~1000 ion cyclotron periods and is not visible on this scale. After the system nonlinearly saturates, the potential structures undergo an oscillatory phase followed by a very slowly evolving static state where the average potential falls linearly over roughly 3 million ion cyclotron periods.

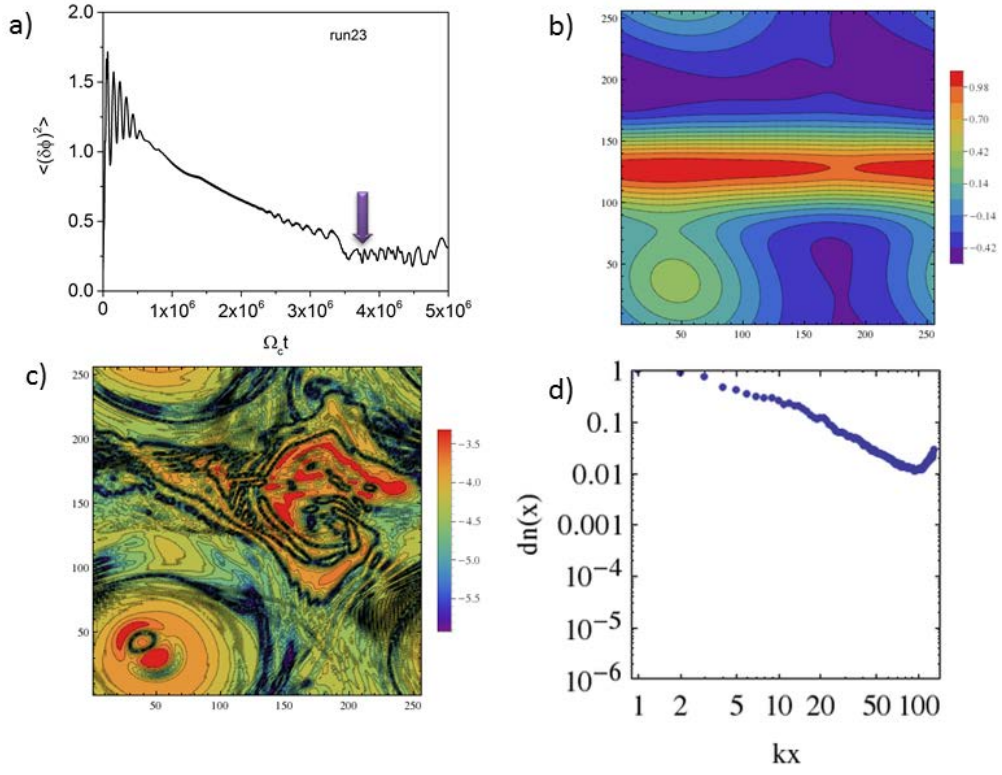

Figure 8. Nonlinear regime of the instability

After $\Omega_{ci}t \approx 3.5\times10^6$, the system begins to rapidly evolve, with nonlinear coupling driving density structures. The (first-order) potential and density at $\Omega_{ci}t \approx 3.7\times10^6$ on the grid is shown in frames (b) and (c). The density contours in frame (c) show evidence of long and short wavelength features. To illustrate this, frame (d) plots the k_x spectrum for the density at this time (averaged in the *y* direction). This spectrum is substantially broader than the k_x density spectrum at earlier times in this simulation. This demonstrates the existence of nonlinear cascade to the short wavelength part of the spectrum. In frame (d) one also can see that the spectrum is of non-Kolmogorov type with different spectral indexes for short and long wavelength parts of the spectrum.

5. CONCLUSIONS

Our study addresses basic problems in the physics of the subauroral geospace associated with the most intense midlatitude space weather events including UHF/GPS and OTHR disruptions that indicate the excitation of short (ion gyroradius-scale) structures. We have explored multispacecraft magnetically-conjugate observations of substorm SAID events near the magnetic equator and in the topside ionosphere. The overall features negate the paradigm of voltage and current generators and agree with a short-circuiting of substorm-injected hot plasma jets over the plasmapasphere and formation of a turbulent boundary layer. Enhanced plasma turbulence within the SAID channel provides anomalous circuit resistivity and magnetic diffusion, as in the well-documented plasmoid-magnetic barrier problem. The suprathermal plasma population is enhanced inside the channel and earthward. The short-circuiting occurs when the cold plasma density exceeds a critical value and the polarization field at the front is shorted out. As a result, the hot electrons are arrested, while the hot ions yet move inward. This provides a natural explanation of the long-known dispersionless auroral boundary. However, we still know little about the underlying mechanism of SAPS, particularly SAPS wave structures (SAPSWS), except that nonlinear effects are significant. SAPSWS appear with RB and RC precipitation, radar clutter, and UHF/GPS scintillations after the onset of substorms. The AFRL hybrid code "Flute" has been modified into a new hydrodynamic code with the ion gyro kinetics for modeling interchange and Kelvin-Helmholtz instabilities in the equatorial and midlatitude ionosphere creating short scale turbulence responsible for UHF/GPS-L band scintillations. Nonlinear system of equations describing the evolution of the instabilities in the presence of finite Larmor radius effects in low- (ionosphere) and high-beta (plasma sheet) plasmas with velocity shear has been derived. A long-time-scale calculation of 2D nonlinear equations shows the formation of nonlinear density structures with a broad wave-number spectrum. The spectrum is substantially broader than the density spectrum at earlier times in this simulation. This demonstrates the existence of nonlinear cascade to the short-wavelength part of the spectrum of non-Kolmogorov type with different spectral indexes for short and long wavelengths.

REFERENCES

[1] Mishin, E. and W. Burke, Stormtime coupling of the ring current, plasmasphere and topside ionosphere: Electromagnetic and plasma disturbances, *J. Geophys. Res.,* **110,** 2005, A07209, 10.1029/2005JA011021, 2005.

[2] Mishin, E. and N. Blaunstein, Irregularities within subauroral polarization stream-related troughs and GPS radio interference at midlatitudes, in: *Midlatitude Ionospheric Dynamics and Disturbances, AGU Monograph* **181**, 2008, pp. 291-295.

[3] Mishin, E. and P. Puhl-Quinn, SAID: Plasmaspheric short circuit of substorm injections, *Geophys. Res. Lett*., **34**, 2007, L24101, doi:10.1029/2007GL031925.

[4] Mishin, E., W. Burke, and A. Viggiano, Stormtime subauroral density troughs: Ion-molecule kinetics effects, *J. Geophys. Res*., **109**, 2004, A10301, 10.1029/2004JA010438.

[5] Puhl-Quinn, P., H. Matsui, E. Mishin, C. Mouikis, L. Kistler, Y. Khotyaintsev, P. Décréau, and E. Lucek, Cluster and DMSP Observations of SAID electric fields, *J. Geophys. Res*., **112**, 2007, A05219, doi.10.1029/2006JA012065.

[6]] Kintner, P. and B. Ledvina, The ionosphere, radio navigation, and global navigation satellite systems, *Adv. Space Res*., **35**, 2005, p. 788.

[7] Retterer, J., Physics-based forecasts of equatorial radio scintillation for the Communication and Navigation Outage Forecasting System (C/NOFS), *Space Weather*, **3**, 2005, S12C03, doi:10.1029/2005SW000146.

[8] Frey, H., S. Mende, V. Angelopoulos, and E. Donovan, Substorm onset observations by IMAGE-FUV, *J. Geophys. Res*., **109**, 2004, A10304, 10.1029/2004JA010607.

[9] Sotnikov, V., et al., Investigation of compressible electromagnetic flute-mode instability in finite-beta plasma in support of Z-pinch and laboratory astrophysics experiments, *Commun. Comp. Phys.,* **4**, 2008, p. 611.

[10] Mishin, E., Plasma Effects in the Interaction of Substorm Injections with the Plasmasphere, *AGU Fall Meeting*, San Francisco, CA, 3-9 December 2012.

[11] Mishin, E., Interaction of substorm injections with the subauroral geospace: 1. Multispacecraft observations of SAID, *J. Geophys. Res. Space Physics*, **118**, 2013, pp. 5782-5796, doi:10.1002/jgra.50548, 2013.

[12] Mishin, E., Turbulent Plasmaspheric Boundary Layer: Observables and Consequences, the *56th Annual Meeting of the APS Division of Plasma Physics*, New Orleans, LA, Nov 2014.

[13] Mishin, E., Plasma Effects in the Interaction of Substorm Injections with the Plasmasphere, *CEDAR*, Seattle, WA, 22-26 June 2014.

[14] Newell, P. and C.-I. Meng, Low altitude observations of dispersionless substorm plasma injections, *J. Geophys. Res*., **92**, 1987, p. 10,063.

[15] Figueiredo, S., E. Karlsson, and G. Marklund, Investigation of subauroral ion drifts and related field-aligned currents and ionospheric Pedersen conductivity distribution, *Annales Geophys*., **22**, 2004, pp. 923-934.

[16] Mishin, E., J. Albert, and O. Santolik, SAID/SAPS-related VLF waves and the outer radiation belt boundary, *Geophys. Res. Lett*., **38**, 2011, L21101, 10.1029/2011GL049613.

[17] Sotnikov, V., T. Kim, J. Lundberg, I. Paraschiv, and T. A. Mehlhorn, Scattering of electromagnetic waves by vortex density structures associated with interchange instability: Analytical and large-scale plasma simulation results, *Phys.Plasmas,* **21**, 2014, 052309, doi: 10.1063/1.4879021.
[18] Sotnikov, V., T. Kim, E. Mishin, T. Genoni, D. Rose and D. Welch, Interchange and Flow Velocity Shear Instabilities in the Presence of Finite Larmor Radius Effects, *C/NOFS Workshop*, Albuquerque, New Mexico, 17-20 June 2013.
[19] Sotnikov, V., T. Kim, J. Lundberg, I. Paraschiv, T.A. Mehlhorn, LSP simulation and analytical results on electromagnetic wave scattering on coherent density structures, *AMOS 2014*, Maui, Hawaii, August 2014.

DISTRIBUTION LIST

DTIC/OCP
8725 John J. Kingman Rd, Suite 0944
Ft Belvoir, VA 22060-6218 1 cy

AFRL/RVIL
Kirtland AFB, NM 87117-5776 2 cys

Official Record Copy
AFRLRVBXI/Dr. Evgeny Mishin 1 cy